Synthesis, characterization and biological studies of Co(II), Ni(II),Cu(II) and Zn(II) complexes with pyrral–L–histidinate

ARTICLE *in* ARABIAN JOURNAL OF CHEMISTRY · APRIL 2012

Impact Factor: 3.73 · DOI: 10.1016/j.arabjc.2010.08.011

2 AUTHORS, INCLUDING:

D. Arish
Vikram Sarabhai Space Centre
19 PUBLICATIONS **96** CITATIONS

Arabian Journal of Chemistry (2012) **5**, 179–186

King Saud University

Arabian Journal of Chemistry

www.ksu.edu.sa
www.sciencedirect.com

ORIGINAL ARTICLE

Synthesis, characterization and biological studies of Co(II), Ni(II), Cu(II) and Zn(II) complexes with pyrral-L-histidinate

D. Arish, M. Sivasankaran Nair *

Department of Chemistry, Manonmaniam Sundaranar University, Tirunelveli 627 012, India

Received 11 July 2010; accepted 18 August 2010
Available online 22 August 2010

KEYWORDS

Schiff base;
IR;
Electronic;
ESR;
Antimicrobial activity

Abstract The Schiff base ligand, pyrral-L-histidinate(L) and its Co(II), Ni(II), Cu(II) and Zn(II) complexes were synthesized and characterized by elemental analysis, mass, molar conductance, IR, electronic, magnetic measurements, EPR, redox properties, thermal studies, XRD and SEM. Conductance measurements indicate that the above complexes are 1:1 electrolytes. IR data show that the ligand is tridentate and the binding sites are azomethine nitrogen, imidazole nitrogen and carboxylato oxygen atoms. Electronic spectral and magnetic measurements indicate tetrahedral geometry for Co(II) and octahedral geometry for Ni(II) and Cu(II) complexes, respectively. The observed anisotropic *g* values indicate the presence of Cu(II) in a tetragonally distorted octahedral environment. The redox properties of the ligand and its complexes have been investigated by cyclic voltammetry. Thermal decomposition profiles are consistent with the proposed formulations. The powder XRD and SEM studies show that all the complexes are nanocrystalline. The *in vitro* biological screening effects of the synthesized compounds were tested against the bacterial species, *Escherichia coli*, *Bacillus subtilis*, *Pseudomonas aeruginosa* and *Staphylococcus aureus*; fungal species,

* Corresponding author. Address: Department of Chemistry, Faculty of Science, Manonmaniam Sundaranar University, Tirunelveli 627 012, Tamil Nadu, India. Mobile: +91 9443540046; fax: +91 462 23334363.
E-mail addresses: arish_d@yahoo.com (D. Arish), msnairchem@rediffmail.com (M.S. Nair).

Peer review under responsibility of King Saud University.
doi:10.1016/j.arabjc.2010.08.011

Production and hosting by Elsevier

Aspergillus niger, *Aspergillus flavus* and *Candida albicans* by the disc diffusion method. The results indicate that complexes exhibit more activity than the ligand. The nuclease activity of the ligand and its complexes were assayed on CT DNA using gel electrophoresis in the presence and absence of H_2O_2.

1. Introduction

Metal ions can simulate some of the features of enzymic active sites by acting as a trap for the Schiff base formed between pyridoxal and amino acids (Casella and Gullotti, 1983; Koh et al., 1996). Transition metal complexes of salicylaldehyde–amino acid Schiff bases are nonenzymatic models for pyridoxal–amino acid systems (Boghaei and Gharagozlou, 2007). Further, the complexes of amino acid Schiff bases possess antibacterial, antifungal and antitumor activities (Sakıyan et al., 2004; Sari and Perihan, 2003; Offiong et al., 2000; Wang et al., 2005). The importance of histidyl residue as a metal ion-binding site in biological systems is well recognized (Deschamps et al., 2003). Many of these systems are enzymes and proteins that contain copper and iron as prosthetic groups. They are mostly involved in oxygen transport, metal storage and transport, electron transfer or oxygen activation (Brill, 1977; Beinert, 1980; Spiro, 1980). In continuation of recent reports from this laboratory on some amino acid Schiff base metal complex systems (Nair and Raj, 2009; Arish and Nair, 2010; Nair et al., 2010), the present paper describes synthesis, characterization and biological studies of a Schiff base ligand derived from pyrrole-2-carboxaldehyde and L-histidine and its Co(II), Ni(II), Cu(II) and Zn(II) complexes.

2. Experimental

2.1. Materials

Pyrrole-2-carboxaldehyde was obtained from Himedia. L-histidine was purchased from Sigma and used without further purification. Calf Thymus (CT) DNA was obtained from Genei, Bangalore. Co(II), Ni(II), Cu(II) and Zn(II) chlorides were Merck samples. All other reagents and solvents were purchased from commercial sources and were of analytical grade.

2.2. Synthesis of Schiff base ligand

Pyrrole-2-carboxaldehyde (0.741 g, 5 mmol) in 20 ml of absolute MeOH and a stirred methanol solution (20 ml) of L-histidine (0.776 g, 5 mmol) containing KOH (0.28 g, 5 mmol) was added dropwise with stirring and refluxed at 50 °C for 8 h. The volume of the resulting solution was reduced to one-third using a rotary evaporator. An air sensitive brownish yellow precipitate was filtered off, washed with anhydrous ether, cold ethanol and then dried *in vacuo* over anhydrous $CaCl_2$. The Schiff base ligand was recrystallized with 80:20 ethanol and water mixture. The yield was found to be 57%.

2.3. Synthesis of the Schiff base metal(II) complexes

To the brownish yellow solution of Schiff base ligand in 20 ml of hot MeOH (5 mmol), a solution of metal(II) chloride in 20 ml of aqueous MeOH (5 mmol) was added dropwise with constant stirring. The reaction mixture was heated under reflux for 2 h and the volume was reduced to half of the initial volume under reduced pressure. The precipitate was filtered off, washed several times with cold EtOH, ether and then dried *in vacuo* over anhydrous $CaCl_2$.

2.4. Physical measurements

Elemental analysis was done using a Perkin-Elmer elemental analyzer. Fast Atom Bombardment (FAB) mass spectra were recorded on a JEOL SX 102/DA-6000 mass spectrometer/data system using argon/xenon (6 kV, 10 mA) as the FAB gas. The metal contents in the complexes were determined by standard EDTA titration (Vogel, 1978). Molar conductance of the complexes was measured in MeOH (10^{-3} M) solutions using a coronation digital conductivity meter. IR spectra were recorded in KBr discs on a JASCO FT/IR-410 spectrometer in the 4000–400 cm^{-1} region. The electronic spectra were recorded on a Perkin-Elmer Lambda-25 UV–Vis spectrometer. Room temperature magnetic measurements were performed on a Guoy's balance by making diamagnetic corrections using Pascal's constant. The X-band ESR spectrum of the Cu(II) complex was recorded on a Varian E112 X-band spectrometer. Cyclic voltammetric measurements were carried out in a Bio-Analytical System (BAS) model CV-50W electrochemical analyzer. The three electrode cells comprised of a reference Ag/AgCl, auxiliary platinum and working glassy electrodes. Tetrabutylammonium perchlorate was used as supporting electrolyte. Thermal analysis was carried out on a SDT Q 600/V8.3 build 101 thermal analyzer with a heating rate of 20 °C/min using N_2 atmosphere. Powder XRD was recorded on a Rigaku Dmax X-ray diffractometer with Cu-Kα radiation ($\lambda_{K\alpha}$ = 1.5406 Å). SEM images were recorded in a Hitachi SEM analyzer.

2.5. Antimicrobial activities

Antibacterial and antifungal activities of the ligand and its complexes were tested *in vitro* against the bacterial species *Escherichia coli* (MSU B05), *Bacillus subtilis* (MSU B06), *Pseudomonas aeruginosa* (MSU B07) and *Staphylococcus aureus* (MSU B08); fungal species, *Aspergillus niger* (MSU F04), *Aspergillus flavus* (MSU F05) and *Candida albicans* (MSU F06) by the disc diffusion method (Bauer et al., 1996). *Amikacin*, *Ofloxacin* and *Ciprofloxacin* were used as standards for antibacterial activity and *Nystatin* was used as standard for antifungal activity. The test organisms were grown on nutrient agar medium in petri plates. The compounds were prepared in DMSO and soaked in a filter paper disc of 5 mm diameter and 1 mm thickness. The discs were placed on the previously seeded plates and incubated at 37 °C and the diameter of inhibition zone around each disc was measured after 24 h for antibacterial and 72 h for antifungal activities. The minimum

inhibitory concentration (MIC) was determined by serial dilution technique.

2.6. Gel electrophoresis

A solution of CT DNA in 0.5 mM NaCl/5 mM Tris–HCl (pH 7.0) gave a ratio of UV absorbance at 260 and 280 nm (A260/A280) of 1.8–1.9, indicating that the DNA was sufficiently free of proteins. Cleavage reactions were run between the metal complexes and DNA, and the solutions were diluted with loading dye using 1% agarose gel. Then 3 μL of ethidium bromide (0.5 μg/ml) was added to the above solution and mixed well. The warmed agarose was poured and clamped immediately with a comb to form sample wells. The gel was mounted into electrophoretic tank; enough electrophoretic buffers were added to cover the gel to a depth of about 1 mm. The DNA sample (30 μM), 50 μM metal complex and 500 μM H_2O_2 in 50 mM Tris–HCl buffer (pH 7.1) were mixed with a loading dye and loaded into the well of the submerged gel using a micropipette. The electric current (50 mA) was passed into the running buffer. After 1–2 h the gel was taken out from the buffer. After electrophoresis, the gel was photographed under UV transluminator (280 nm) and documented.

3. Results and discussion

The analytical data and physical properties of the Schiff base ligand (L) and its complexes are listed in Table 1. The Schiff base ligand is soluble in common organic solvents such as EtOH, $CHCl_3$ and MeOH. The proposed structure of the Schiff base ligand is given in Fig. 1. The air sensitive Schiff base ligand is not stable for long under ordinary laboratory conditions. It is highly affected by direct sunlight and is decomposed within 1 week. Hence, it was used, as prepared, without delay. However, the resulting metal complexes were found to be stable at room temperature and insoluble in common solvents such as EtOH, $CHCl_3$, MeOH and water but soluble in DMF and DMSO. The elemental analysis data (Table 1) confirmed that the complexes have a 1:1 molar ratio between the metal and the Schiff base ligand. The molar conductance of all the complexes was measured in DMSO using 10^{-3} M solutions at room temperature. The conductance (Table 1) values indicate that all the complexes are in 1:1 electrolytic nature (Geary, 1971). In addition, the presence of uncoordinated chloride is also confirmed by the silver nitrate test (Vogel, 1978).

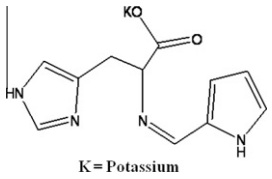

Figure 1 Proposed structure of the Schiff base ligand.

3.1. Mass spectra

The mass spectrum of the Schiff base ligand shows a well-defined molecular ion peak at $m/z = 270$ (relative intensity = 16%), which coincides with a formula weight of the Schiff base. The spectrum of the ligand shows a series of peaks at m/z 231 (100%), 153 (58%), 107 (72%), 89 (60%) and 56 (53%) corresponding to its various fragments. The mass spectra of Co(II), Ni(II), Cu(II) and Zn(II) complexes show a molecular ion peak (M^+) at m/z 344 (18%), 414 (12%), 420 (23%) and 350 (28%), respectively, suggesting the complex to be monomeric, confirming the stoichiometry of the metal to ligand ratio to be 1:1 in all the complex systems.

3.2. IR spectra

The important IR spectral data of the Schiff base ligand and its complexes are given in Table 2. The IR spectrum of the free Schiff base ligand exhibits a sharp band at 1632 cm^{-1}, due to the azomethine group ν(C═N). On complexation this band was shifted to a lower frequency in the ~1625–1618 cm^{-1} range indicating the coordination of the azomethine nitrogen atom to the metal ion. The IR spectrum of the Schiff base ligand exhibits a broad band centered at 1605 cm^{-1} due to asymmetric carboxyl $\nu_{as}(COO^-)$-stretching modes, which is probably broadened because of an overlap with aromatic ring carbon stretching and imidazole ring imido nitrogen-stretching frequency (Pessoa et al., 1998; Nakamoto, 1978). In addition, the band at 1410 cm^{-1} can be ascribed to the symmetric carboxyl $\nu_s(COO^-)$ group. During complexation they were shifted to lower frequency by ~5–16 cm^{-1} indicating the linkage between the metal ion and carboxylato oxygen atom. The

Table 1 Analytical and physical data of the ligand and its complexes.

Compound	Empirical formula	Color	Elemental analysis Found (calcd) (%)				Molar conductance (Ω^{-1} cm^2 mol^{-1})
			C	H	N	M	
L	$KC_{11}H_{11}N_4O_2$	Brown	48.72 (48.87)	4.23 (4.10)	20.08 (20.73)	–	–
$[CoL(H_2O)]Cl$	$CoC_{11}H_{13}N_4O_3Cl$	Violet	38.16 (38.45)	3.97 (3.81)	16.04 (16.30)	17.11 (17.15)	90
$[NiL(H_2O)_3]Cl{\cdot}2H_2O$	$NiC_{11}H_{21}N_4O_7Cl$	Dark green	31.72 (31.80)	5.01 (5.09)	12.97 (13.49)	14.03 (14.13)	82
$[CuL(H_2O)_3]Cl{\cdot}2H_2O$	$CuC_{11}H_{21}N_4O_7Cl$	Green	31.32 (31.43)	4.95 (5.04)	12.92 (13.33)	15.23 (15.12)	97
$[ZnL(H_2O)]Cl$	$ZnC_{11}H_{13}N_4O_3Cl$	Yellow	36.99 (37.14)	3.93 (3.74)	15.97 (16.00)	18.44 (18.68)	95

Table 2 IR spectral data of the ligand and its complexes (cm^{-1}).

Compound	[a]$\nu_{azo.}$(C═N)	$\nu_{as}(COO^-)$ [b]$\nu_{imida\ ring}$(C═N)	$\nu_s(COO^-)$	[c]$\nu(H_2O)$	ν(M–O)	ν(M–N)
L	1632	1605	1410	–	–	–
$[CoL(H_2O)]Cl$	1624	1592	1398	3325	530	412
$[NiL(H_2O)_3]Cl{\cdot}2H_2O$	1622	1595	1398	3330	545	423
$[CuL(H_2O)_3]Cl{\cdot}2H_2O$	1618	1595	1397	3325	540	420
$[ZnL(H_2O)]Cl$	1625	1597	1400	3320	547	415

[a] Azomethine stretching frequency.
[b] Imidazole ring imido nitrogen stretching frequency.
[c] Water molecule stretching frequency.

large difference between $\nu_{as}(COO^-)$ and $\nu_s(COO^-)$ (~200 cm^{-1}) indicates the monodentate-binding nature of the carboxylato group in the complexes (Nakamoto, 1978; Deacon and Phillips, 1980). The presence of a water molecule in the complexes is indicated by the very broad absorption band centered at ~3330 cm^{-1} (Hosny, 1998). In the lower frequency region the weak bands observed at 547–530 and 423–412 cm^{-1} have been assigned to the ν(M–O) and ν(M–N) vibrations, respectively (Nakamoto, 1978; Ouf et al., 2010). Thus the IR spectrum indicates that the Schiff base ligand acts as a tridentate N_2O donor involving azomethine nitrogen, imidazole nitrogen and carboxylato oxygen donor atoms.

3.3. Electronic spectra and magnetic measurements

The electronic spectral and magnetic moment data of the complexes are given in Table 3. The electronic spectrum of free Schiff base ligand shows a broad band at 367 nm, which is assigned to the π–π* transition of the azomethine (>C═N–) chromophore. On complexation this band was shifted to lower wavelengths, suggesting the coordination of azomethine nitrogen to the central metal ion. The electronic spectrum of tetrahedral Co(II) complexes is reported to have only one absorption band in the visible region due to the $^4A_2(F) \rightarrow {}^4T_1(P)$ transition (Lever, 1984). The spectrum of the present Co(II) complex has only one band in the visible region at 568 nm (Table 1), which indicates tetrahedral geometry for the complex. The electronic spectrum of the Ni(II) complex shows three bands at ~1100, 720 and 420 nm (Fig. 8), respectively, due to the metal-based transitions $^3A_2g\ (F) \rightarrow {}^3T_2g\ (F)$, $^3A_2g\ (F) \rightarrow {}^3T_1g\ (F)$ and $^3A_2g\ (F) \rightarrow {}^3T_1g(P)$, indicating octahedral orientation of donor centers around the metal ion (Rosu et al., 2010). The Cu(II) complex exhibits a broad absorption at 800 nm and a weak shoulder at 430 nm. This is due to d–d transitions, which correspond to the $^2Eg \rightarrow {}^2A_1g$ and $^2Eg \rightarrow {}^2B_1g$ transitions, respectively (Nag et al., 2005). This supports the distorted octahedral structure for the Cu(II) complex.

Table 3 Electronic and magnetic moment data of metal complexes.

Compound	Electronic spectra wavelength (nm)	Magnetic moment (BM)	Geometry
L	220, 250, 367	–	–
$[CoL(H_2O)]Cl$	568	4.17	Tetrahedral
$[NiL(H_2O)_3]Cl{\cdot}2H_2O$	420, 720, 1100	3.07	Octahedral
$[CuL(H_2O)_3]Cl{\cdot}2H_2O$	430, 800	1.98	Octahedral

The Co(II) complex has a magnetic moment of 4.17 BM (Table 1), which is in agreement with the reported value for tetrahedral Co(II) complexes (Sevagapandian et al., 2000). The present Ni(II) complex shows a magnetic moment value of 3.07 within the range of 2.9–3.3 BM (Sharaby, 2007) suggesting octahedral environment. The Cu(II) complex shows a magnetic moment value of 1.98 BM, which is slightly higher than the spin-only value 1.73 BM expected for the distorted octahedral Cu(II) complexes (Mohamed et al., 2009).

3.4. Electrochemical studies

All cyclic voltammograms were recorded in acetonitrile solution at a scan rate of 100 mV s^{-1} in the potential range +2.0 to −2.0 V. The Schiff base ligand and Zn(II) complex have not shown any peaks in this potential range under similar conditions. The cyclic voltammogram of the Co(II) complex shows a well-defined redox process corresponding to the formation of the quasi-reversible Co(II)/Co(I) couple. The cathodic peak at −0.848 V versus Ag/AgCl and the associated anodic peak at −0.640 V correspond to the Co(II)/Co(I) couple. The peak to peak separation (ΔE_p = 0.208 V) indicates a quasi-reversible one-electron transfer process. The redox property of the Ni(II) complex displayed an anodic and associated cathodic peaks at −0.898 and −0.506 V, respectively, corresponding to the formation of the quasi-reversible (ΔE_p = 392) one-electron reduction Ni(II)/Ni(I) couple. The Cu(II) complex displayed a cathodic peak at −0.868 V versus Ag/AgCl with the corresponding anodic wave at −0.663 V on the reverse scan (Fig. 2). The peak separation value (ΔE_p = 205 V) indicates a totally quasi-reversible character for the one-electron transfer reaction of metal-based Cu(II)/Cu(I) couple.

3.5. ESR studies

The ESR spectra of the Cu(II) complex (Fig. 3) in a polycrystalline state at room temperature exhibited anisotropic signals with g values $g_{\|}$ = 2.13 and $g_{\perp}$ = 2.03, respectively, which is characteristic for the axial symmetry of Cu(II) complexes (Chandra and Gupta, 2004; Rajalakshmi et al., 2008). The $g_{\|}$ and $g_{\perp}$ values are closer to 2 and $g_{\|} > g_{\perp}$. This suggests a tetragonal distortion around Cu(II) corresponding to elongation along the four-fold symmetry Z-axis (Mohamed et al., 2009). The trend $g_{\|}(2.13) > g_{\perp}(2.03) > g_e(2.0023)$ shows that

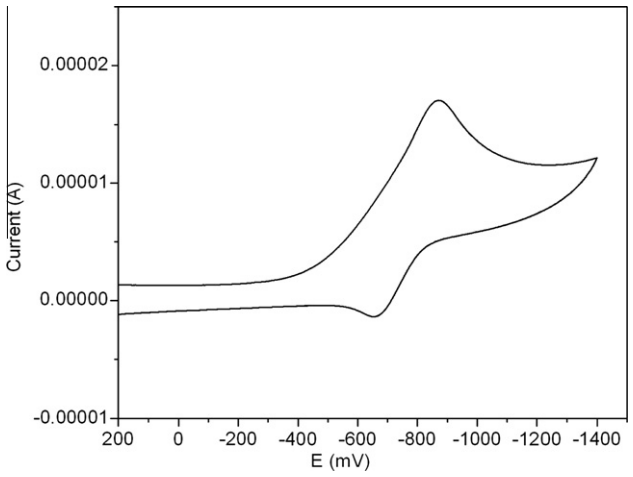

Figure 2 Cyclic voltammogram of the $[CuL(H_2O)_3]Cl{\cdot}2H_2O$ complex.

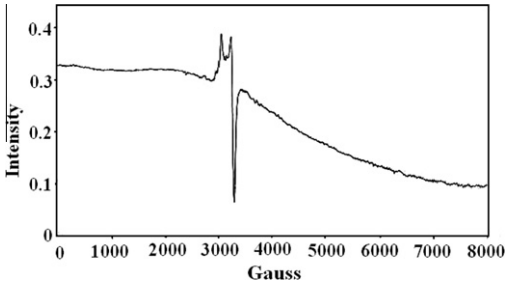

Figure 3 ESR spectrum of the $[CuL(H_2O)_3]Cl{\cdot}2H_2O$ complex.

the unpaired electron is localized in the $dx^2 - y^2$ orbital of the Cu(II) ions in the complex (Krishna et al., 2008). In addition, an exchange coupling interaction between two Cu(II) ions is explained by Hathaway expression $G = (g_{\|} - 2)/(g_{\perp} - 2)$ (Hathaway and Tomlinson, 1970). If the value $G > 4.0$, the exchange interaction is negligible and if $G < 4.0$, a considerable exchange coupling is present in the solid complex. In the present Cu(II) complex, the '*G*' value (4.33) is >4 indicating that there is no interaction in the complex. Moreover, the absence of a half field signal at 1600 G corresponding to $\Delta M = \pm 2$ transitions indicates the absence of any Cu–Cu interaction in the complex (Gaballa et al., 2007). Kivelson and Neiman (1961) have shown that for an ionic environment $g_{\|}$ is 2.3 or larger, but for a covalent environment $g_{\|}$ is less than 2.3. The $g_{\|}$ value for the present complex is 2.13, indicating a significant degree of covalency in the metal–ligand bond.

3.6. Thermogravimetric studies

Thermogravimetric studies have been made in the temperature range 25–900 °C. The thermal stability data of the complexes are listed in Table 4. Thermal decomposition curves of the Co(II) and Zn(II) complexes show a similar sequence of two decomposition steps. In the first step, Co(II) and Zn(II) complexes lost one molecule of coordinated water and a chloride ion as HCl gas between 155 and 270 °C, which is an endothermic process as the DTA curve indicates. The next exothermic step of the thermal degradation that occurs between 360 and 615 °C corresponds to the removal of organic ligand moiety leaving a metal oxide residue. The thermal decomposition of the Ni(II) and Cu(II) complexes occurs in three stages. The first thermal dehydration begins at 50 °C and ends at 140 °C with an endothermic peak. The observed mass loss is attributed to the decomposition of two lattice water molecules. The second endothermic step of the thermal degradation that occurs between 156 and 310 °C corresponds to the decomposition of the three coordinated water molecules and a chloride ion as HCl gas. Above this temperature a gradual weight loss continues up to 630 °C, which corresponds to the decomposition of the Schiff base ligand from the metal chelate. The horizontal thermal curve observed above 630 °C corresponds to a metal oxide residue. The thermal analysis curves of the Cu(II) complex are given in Fig. 4. Based on the above results, the proposed structure of the complexes is given in Fig. 5.

Table 4 Thermogravimetric data of Co(II), Ni(II), Cu(II) and Zn(II) complexes.

Complex	Temperature (°C)	DTA peak (°C)	% weight loss Obs. (calcd)	Process
$[CoL(H_2O)]Cl$	155–270	253 endo 290 endo	15.70 (15.54)	Loss of coordinated water molecule and chloride ion
	380–610	420 exo	62.21 (62.50)	Loss of organic moieties
	>610	548 exo	Residue 22.09 (21.80)	CoO
$[NiL(H_2O)_3]Cl{\cdot}2H_2O$	60–130	125 endo	8.48 (8.69)	Loss of lattice water molecule
	156–310	267 endo	21.79 (22.61)	Loss of coordinated water molecule and chloride ion
	325–645	405 exo	51.31 (51.73)	Loss of organic moieties
	>645	570 exo	Residue 18.42 (17.87)	NiO
$[CuL(H_2O)_3]Cl{\cdot}2H_2O$	52–140	120 endo	8.89 (9.28)	Loss of lattice water molecule
	160–307	265 endo	21.26 (21.30)	Loss of coordinated water molecule and chloride ion
	330–630	400 exo	50.73 (51.19)	Loss of organic moieties
	>630	575 exo	Residue 19.12 (18.80)	CuO
$[ZnL(H_2O)]Cl$	160–270	255 endo 291 endo	15.44 (15.28)	Loss of coordinated water molecule and chloride ion
	368–615	420 exo	61.54 (61.42)	Loss of organic moieties
	>615	555 exo	Residue 23.02 (22.85)	ZnO

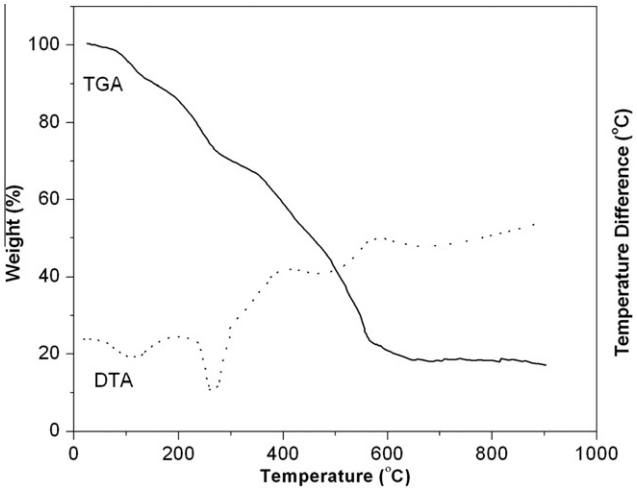

Figure 4 Thermal analyses curves of the $[CuL(H_2O)_3]Cl{\cdot}2H_2O$ complex.

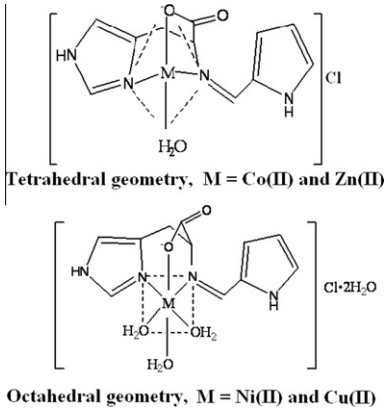

Figure 5 Proposed structure of the metal complexes.

3.7. Powder XRD and SEM

The powder XRD patterns of Co(II), Ni(II), Cu(II) and Zn(II) complexes were recorded over the 2θ = 0–80 Å range and are shown in Fig. 6. From the data, all the complexes show sharp peaks indicating their crystalline nature. The average crystallite sizes of the complexes d_{XRD} were calculated using Scherrer's formula (Dhanaraj and Nair, 2009). The Co(II), Ni(II), Cu(II) and Zn(II) complexes have an average crystallite size of 89, 56, 16 and 39 nm, respectively, suggesting that the complexes are in a nanocrystalline phase.

The SEM micrographs of the Co(II), Ni(II), Cu(II) and Zn(II) complexes are given in Fig. 7. The SEM pictures of the complexes show different morphological structures and the presence of small grains in the nanometer range. The Co(II) complex displays closely packed cauliflower-like morphological structures, while Ni(II) complex has a broken-stone like surface morphology. The SEM picture of the Cu(II) complex exhibits clusters of cotton like morphology and the presence of small grains are uniformly arranged. The Zn(II) complex has small ice bar like morphology. The average grain size found from SEM shows that the complexes are polycrystalline with nano sized grains.

3.8. Antimicrobial activity

The results of the antimicrobial activities are summarized in Table 5. The standard error for the experiment is ±0.001 cm and the experiment is repeated three times under similar conditions. DMSO is used as negative control and *Amikacin*, *Ofloxacin* and *Ciprofloxacin* were used as positive standards for antibacterial and *Nystatin* for antifungal activities. The results show that the metal chelates are more active than the starting materials and the free ligands. The antimicrobial

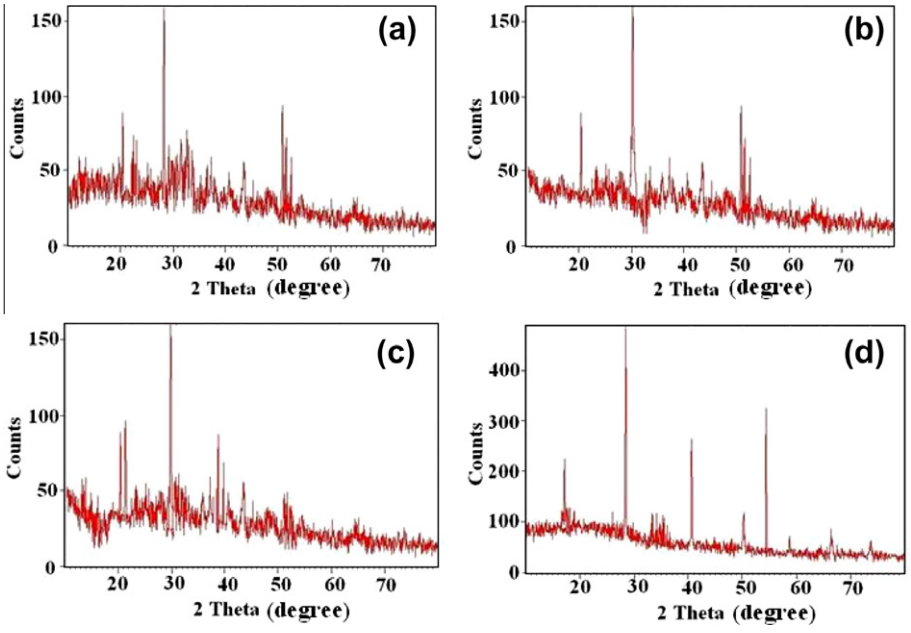

Figure 6 XRD patterns of (a) $[CoL(H_2O)]Cl$, (b) $[NiL(H_2O)_3]Cl{\cdot}2H_2O$, (c) $[CuL(H_2O)_3]Cl{\cdot}2H_2O$, (d) $[ZnL(H_2O)]Cl$ complexes.

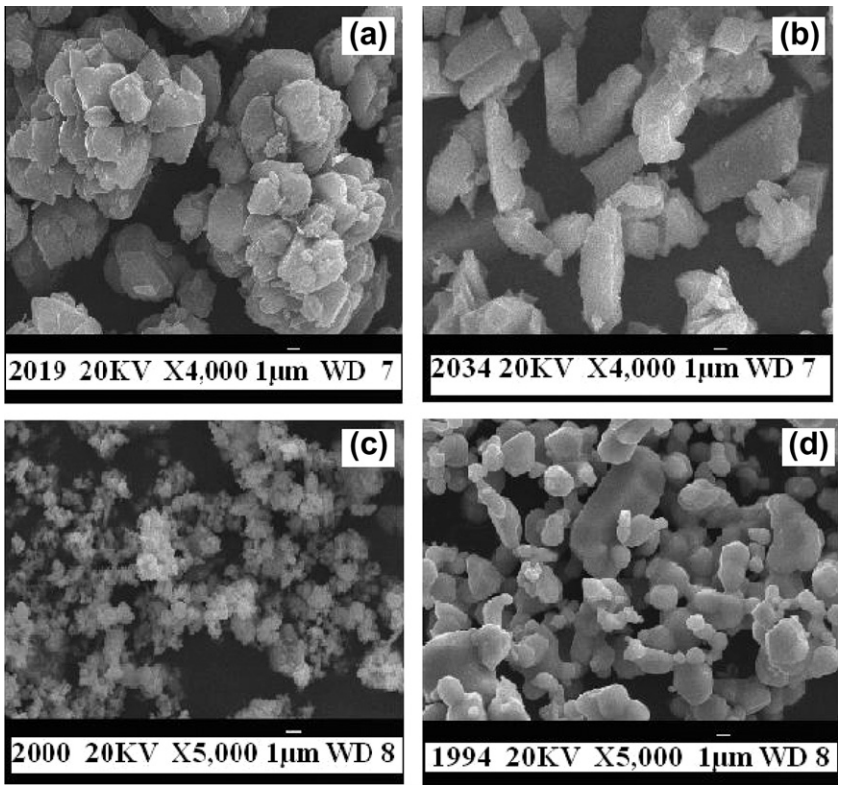

Figure 7 SEM images of (a) $[CoL(H_2O)]Cl$, (b) $[NiL(H_2O)_3]Cl{\cdot}2H_2O$, (c) $[CuL(H_2O)_3]Cl{\cdot}2H_2O$, (d) $[ZnL(H_2O)]Cl$ complexes.

Table 5 *In vitro* antimicrobial activity (MIC, µg/ml) of the compounds and standard reagents.

Compound	Bacterial species				Fungal species		
	E. coli	*B. subtilis*	*P. aereuguinosa*	*S. aureus*	*A. niger*	*A. flavus*	*C. albicans*
L	20	80	75	>100	25	>100	80
$[CoL(H_2O)]Cl$	18	75	20	50	35	26	15
$[NiL(H_2O)_3]Cl{\cdot}2H_2O$	15	14	10	25	34	15	15
$[CuL(H_2O)_3]Cl{\cdot}2H_2O$	05	18	32	28	12	25	08
$[ZnL(H_2O)]Cl$	>100	35	24	30	22	75	75
Amikascin[a]	05	05	04	05	–	–	–
Ciprofloxacin[a]	05	05	05	05	–	–	–
Ofloxacin[a]	10	02.5	02.5	05	–	–	–
Nystatin[a]	–	–	–	–	06	06	05

[a] Standards.

activity of the complexes is often greater than those of the corresponding free ligands, explained on the basis of Overtone's concept and chelation theory (Priya et al., 2009). The Schiff base ligand has good activity against the bacterial strain *E. coli* whereas all the complexes exhibited excellent *in vitro* antibacterial activity against Gram-positive and Gram-negative organisms. Among the complexes, Ni(II) and Cu(II) complexes were highly active against both Gram-positive and Gram-negative organisms and this antibacterial effect is equal to that of some antibiotics. The Co(II) complex was found to be highly active towards *E. coli*.

The fungicidal screening shows that *C. albicans* was inhibited by Co(II), Ni(II) and Cu(II) complexes having MIC values 15, 15 and 08, respectively. The free Schiff base ligand was more active than some of its metal complexes against the fungi *A. niger*. The Ni(II) and Cu(II) complexes show good activity against all the tested fungal strains (MIC < 100). The activity order of the synthesized compounds is as follows: Cu(II) > Ni(II) > Co(II) > Zn(II) > L.

3.9. Nuclease activity

Gel electrophoresis experiments using CT DNA were performed with the ligand and its complexes in the presence and absence of H_2O_2 as an oxidant. The results (Fig. 8) indicate that all the complexes can interact with CT DNA in the presence of H_2O_2. However, Ni(II) and Cu(II) complexes can cleave DNA effectively compared to other systems. Probably

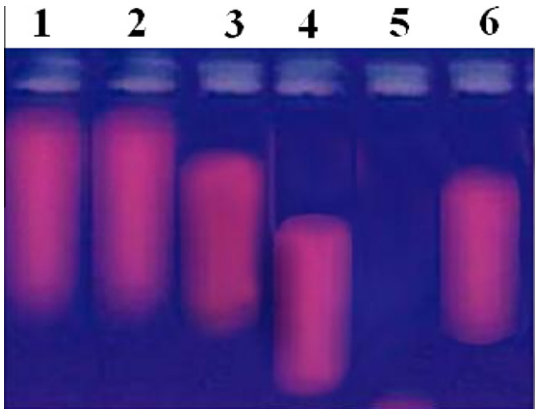

Figure 8 Gel electrophoresis diagram for the reaction done in the control experiment with an incubation time of 60 min at 30 °C in dark condition: lane 1: DNA + H_2O_2; lane 2: DNA + ligand + H_2O_2; lane 3: DNA + $[CoL(H_2O)]Cl$ + H_2O_2; lane 4: DNA + $[NiL(H_2O)_3]Cl{\cdot}2H_2O$; lane 5: DNA + $[CuL(H_2O)_3]Cl{\cdot}2H_2O$ + H_2O_2; lane 6: DNA + $[ZnL(H_2O)]Cl$ + H_2O_2.

this is due to the formation of the redox couple of the metal ions and its behavior. The redox cycling between M(II) and M(I) can catalyze the production of highly reactive hydroxyl radicals. These hydroxyl radicals participate in the oxidation of the deoxyribose moiety, followed by the hydrolytic cleavage of the sugar-phosphate backbone. It is observed that most cleavage cases are caused by the metal ions reacting with H_2O_2 to produce diffusible hydroxyl radicals or molecular oxygen, which may damage DNA through a Fenton type chemistry (Babu et al., 2007). The presence of a smear in the gel diagram indicates the presence of a radical cleavage. In addition, the nuclease activity of the complexes has also been investigated in the absence of the oxidant H_2O_2. Moreover, no effect was observed indicating the involvement of hydroxyl radicals in the cleavage process.

4. Conclusion

Co(II), Ni(II), Cu(II) and Zn(II) complexes with N_2O donor Schiff base ligand derived from pyrrole-2-carboxaldehyde and L-histidine were synthesized. A comparative study of their physico-chemical properties have been made through elemental analysis, molar conductance, mass, IR, electronic spectra, magnetic moment, ESR, CV, TG/DTA, powder XRD and SEM. The conductance data indicate that all the complexes are 1:1 electrolytes. The IR data reveal that the Schiff base ligand pyrral-L-histidinate coordinates through the azomethine nitrogen, imidazole nitrogen and carboxylato oxygen atoms. A tetrahedral geometry for Co(II) and Zn(II) complexes and octahedral/distorted octahedral geometry were assigned for Ni(II) and Cu(II) complexes. The ESR spectrum of the Cu(II) complex reveals its tetragonally distorted octahedral geometry. The thermal decomposition of the Co(II) and Zn(II) complexes is a two-stage process while the Ni(II) and Cu(II) complexes displayed a three-step process. Powder XRD results show that the complexes are of crystalline nature. The SEM image of Co(II) complex exhibits cauliflower-like morphological structures. Ni(II) and Cu(II) complexes were found to be more active against most of the microbes and they effectively cleaved CT DNA in the presence of an oxidant.

Acknowledgment

One of the authors (D. Arish) is grateful to National Testing Service, India, CIIL, Mysore for providing the fellowship.

References

Arish, D., Nair, M.S., 2010. J. Coord. Chem. 63, 1619.
Babu, M.S.S., Reddy, K.H., Pitchika, G.K., 2007. Polyhedron 26, 572.
Bauer, A.W., Kirby, W.M.M., Sherries, J.C., Truck, M., 1996. Am. J. Clin. Pathol. 45, 493.
Beinert, H., 1980. Coord. Chem. Rev. 33, 55.
Boghaei, D.M., Gharagozlou, D., 2007. J. Coord. Chem. 60, 339.
Brill, A.S., 1977. Transition Metals in Biochemistry. Springer-Verlag, New York (Chapter 2).
Casella, L., Gullotti, M., 1983. J. Am. Chem. Soc. 105, 803.
Chandra, S., Gupta, L.K., 2004. Spectrochim. Acta A 60, 1563.
Deacon, G.B., Phillips, R.J., 1980. Coord. Chem. Rev. 33, 227.
Deschamps, P., Kulkarni, P.P., Sarkar, B., 2003. Inorg. Chem. 42, 7366.
Dhanaraj, C.J., Nair, M.S., 2009. Eur. Polym. J. 45, 565.
Gaballa, A.S., Asker, M.S., Barakat, A.S., Teleb, S.M., 2007. Spectrochim. Acta A 67, 114.
Geary, W.J., 1971. Coord. Chem. Rev. 7, 81.
Hathaway, B.J., Tomlinson, G.A.A., 1970. Coord. Chem. Rev. 5, 1.
Hosny, W.M., 1998. Synth. React. Inorg. Met. Org. Chem. 28, 1029.
Kivelson, D., Neiman, R., 1961. J. Chem. Phys. 35, 149.
Koh, L.L., Ranford, J.O., Robinson, W.T., Svensson, J.O., Tan, A.L.C., Wu, D., 1996. Inorg. Chem. 35, 6466.
Krishna, P.M., Reddy, K.H., Pandey, J.P., Siddavattam, D., 2008. Transition Met. Chem. 33, 661.
Lever, A.B.P., 1984. Inorganic Electronic Spectroscopy, second ed. Elsevier, New York.
Mohamed, G.G., Omar, M.M., Ibrahim, A.A., 2009. Eur. J. Med. Chem. 44, 4801.
Nag, J.K., Pal, S., Sinha, C., 2005. Transition Met. Chem. 30, 523.
Nair, M.S., Raj, C.R.S., 2009. J. Coord. Chem. 62, 2903.
Nair, M.S., Raj, C.R.S., Arish, D., Kumari, S., 2010. J. Indian Chem. Soc. 87, 729.
Nakamoto, K., 1978. Infra-Red and Raman Spectra of Inorganic and Coordination Compounds, third ed. John Wiley & Sons, New York.
Offiong, O.E., Nfor, E., Ayi, A.A., Martelli, S., 2000. Transition Met. Chem. 25, 369.
Ouf, A.E.L., Ali, M.S., Saad, E.M., Mostafa, S.I., 2010. J. Mol. Struct. 973, 69.
Pessoa, J.C., Duarte, M.T., Gillard, R.D., Madeira, C., Matias, P.M., Tomaz, I., 1998. J. Chem. Soc., Dalton Trans., 4015.
Priya, N.P., Arunachalam, S.V., Sathya, N., Chinnusamy, V., Jayabalakrishnan, C., 2009. Transition Met. Chem. 34, 437.
Rajalakshmi, V., Vijayaraghavan, V.R., Varghese, B., Raghavan, A., 2008. Inorg. Chem. 47, 5821.
Rosu, T., Negoiu, M., Pasculescu, S., Pahontu, E., Poirier, D., Gulea, A., 2010. Eur. J. Med. Chem. 45, 774.
Sakıyan, I., Glu, E.L.G., Arslan, S., Sari, N., Sakıyan, N., 2004. Biometals 17, 115.
Sari, N.E., Perihan, G., 2003. Transition Met. Chem. 28, 468.
Sevagapandian, S., Rajagopal, G., Nehru, K., Athappan, P., 2000. Transition Met. Chem. 25, 388.
Sharaby, C.M., 2007. Spectrochim. Acta A 66, 1271.
Spiro, T.G., 1980. Metal Ion Activation of Dioxygen. Wiley, New York.
Vogel, A.I., 1978. A Textbook of Quantitative Inorganic Analysis Including Elementary Instrumental Analysis, fourth ed. Longman, London.
Wang, M.Z., Meng, Z.X., Liu, B.L., Cai, G.L., Zhang, C.L., Wang, X.Y., 2005. Inorg. Chem. Commun. 8, 368.